Pixelated mask spatial carrier phase shifting interferometry algorithms and associated errors

Bradley T. Kimbrough

In both temporal and spatial carrier phase shifting interferometry, the primary source of phase calculation error results from an error in the relative phase shift between sample points. In spatial carrier phase shifting interferometry, this phase shifting error is caused directly by the wavefront under test and is unavoidable. In order to minimize the phase shifting error, a pixelated spatial carrier phase shifting technique has been developed by 4D technologies. This new technique allows for the grouping of phase shifted pixels together around a single point in two dimensions, minimizing the phase shift change due to the spatial variation in the test wavefront. A formula for the phase calculation error in spatial carrier phase shifting interferometry is derived. The error associated with the use of linear N-point averaging algorithms is presented and compared with those of the pixelated spatial carrier technique.

OCIS codes: 120.0120, 120.3180, 120.3940, 120.5050.

1. Introduction

Determination of the spatial variations of optical phase is of primary importance in the fields of optical testing and metrology, optical recording of wavefronts, optical information processing, and adaptive optics. There exist several techniques for the encoding of spatial phase modulation in fringe patterns and the subsequent analysis of these fringe patterns for a quantitative determination of phase.[1] The two primary groups of fringe pattern analysis techniques are temporal phase measurement (sometimes known as the phase shifting method) and spatial phase measurement (which is also called the spatial carrier method).

Temporal phase measurement is a well-established method for measuring the optical wavefront phase.[2] In this technique, three or more interferogram intensity profiles are recorded. For each recording, there is a different relative phase between the test and the reference beams. There are two major limitations to temporal phase measurement. The first limitation is its extreme sensitivity to vibration and turbulence. The second limitation, which is the largest source of error in vibration free environments, results from an inability to precisely control the relative phase shifts between interferograms.[3] A majority of the scholarship in temporal phase measurement has been focused on the analysis and development of algorithms that are less sensitive to phase shifting errors.[4–9]

Spatial phase measurement utilizes a single interferogram to extract phase information.[10] In this technique, a spatial carrier, typically in the form of high frequency tilt fringes, is applied to the interferogram. The intensity profile of the modulated spatial carrier interferogram is recorded and then analyzed in one of two spatial phase measurement techniques to determine the phase. In the first technique, the data are processed in the Fourier domain.[11] Fourier domain processing will not be discussed in this paper, but it should be mentioned that the Fourier domain approach is not sensitive to the phase shift errors described here, because it makes no *a priori* assumptions about the phase increment between pixels. In the second technique, data are processed in the spatial domain. The primary advantage of the spatial phase measurement technique over the temporal phase measurement is that only one image is required. This allows measurements to be taken in adverse conditions or of dynamic events.

The spatial carrier phase shifting method is a spatial domain processing technique and is a direct application of temporal phase shifting algorithms to spatial phase measurement.[12] This method assumes that the phase difference between pixels remains constant over a small interval, and is equal to the fringe

The author (bkimbrough@optics.arizona.edu) is with the College of Optical Sciences, University of Arizona, Tucson, Arizona 85721.

Received 27 October 2005; revised 19 January 2006; accepted 21 January 2006; posted 24 January 2006 (Doc. ID 65590).

0003-6935/06/194554-09$15.00/0

carrier frequency. The largest source of error in this method results from the assumption of constant phase shift between the pixels in an interval.[13] Because the phase shift between pixels is a result of both the spatial carrier phase and the test wavefront phase, the assumption of constant phase shift is valid only for wavefronts with small deviations. The resulting error is analogous to the phase shift calibration error in temporal phase shifting. Just as in temporal phase shifting, application of algorithms less sensitive to detuning can minimize this error. However, these detuning insensitive algorithms generally involve more sample points, making the assumption of constant phase slope across the sample interval more difficult to maintain.

In order to minimize phase calibration error, a pixelated spatial carrier phase shifting technique has been developed by 4D technology.[14] In this technique, the relative phase between carrier and test wavefront is modified on a pixel by pixel basis. The phase shifts are produced with a wire grid polarizing array placed at a point just prior to detection. This method allows for the grouping of phase shifted pixels together around a single point in two dimensions, minimizing the phase shift change due to the spatial variation in the test wavefront. An analysis of the wavefront induced errors in the pixelated spatial carrier technique along with a comparison to the performance of standard linear algorithms is the subject of this paper.

This paper begins with an analysis of the wavefront induced errors in spatial carrier phase shifting interferometry. A general error formula is derived that is valid for the N-point averaging algorithms, class A, outlined by Schmit and Creath,[7] and contains no approximations. A simplification of this formula is then derived for the case of a wavefront with tilt and comparisons made with results obtained from computer simulations. The pixelated spatial carrier technique is then introduced along with the circular-4, circular-9, stacked-4, and stacked-9 algorithms. The general error formula will be shown to be valid for use with these new algorithms, and an analytic solution expressing the error as a function of tilt will be derived. These analytical results will also be compared with those obtained through a computer simulation. Finally, a comparison will be made between the circular and stacked algorithms and the linear algorithms.

2. General Error Formula Derivation

In spatial carrier phase shifting, the wavefront being measured (the test wavefront) modulates the spatial carrier (the reference wavefront), altering the nominal phase shift between pixels and resulting in a phase calculation error. This error is both wavefront and algorithm dependent. In this section, a formula for the wavefront dependent phase calculation error is derived for the N-point averaging algorithms.

The N-point averaging algorithms used in this analysis are a class of error compensating algorithms based upon the conventional 4-point method.[7] The conventional 4-point algorithm is

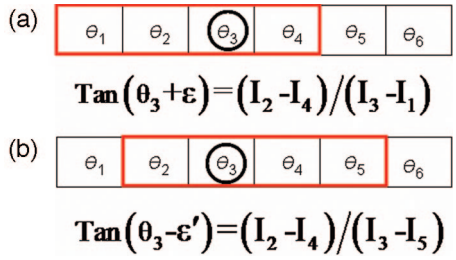

Fig. 1. (Color online) Calculating θ_3 using shifted data sets.

$$\tan(\theta) = \frac{I_2 - I_4}{I_3 - I_1}, \tag{1}$$

where I_n is the intensity at point n, and the phase shift between points is $\pi/2$ radians. Derivation of the 5-point algorithm from the 4-point algorithm is as follows: Figure 1(a) shows a row of six pixel elements, where the phase at each element is θ_n, n being the pixel number. In addition to this wavefront phase, there is a carrier phase of $n\pi/2$ at each point. Using the 4-point formula of Eq. (1) and the intensity values corresponding to points 1–4, the phase at $n = 3$ is determined by

$$\tan(\theta_3 + \varepsilon) = (I_2 - I_4)/(I_3 - I_1), \tag{2}$$

where ε is the error in the phase calculation.

The phase at $n = 3$ can also be calculated by using the intensity values at points 2–5 as shown in Fig. 1(b). The formula in this case is

$$\tan(\theta_3 - \varepsilon') = (I_2 - I_4)/(I_3 - I_5), \tag{3}$$

where ε' is the error in the phase calculation. Note that in Eq. (2) ε is added to the phase, whereas in Eq. (3) ε' is subtracted. Both calculations have approximately the same error, but of opposite sign. An average of the results of these two calculations will then significantly reduce the error. Schwider *et al.*[3] pointed out that, instead of taking two separate measurements and averaging the results, one could simply average the numerator and the denominators in Eqs. (2) and (3) resulting in the 5-point formula:

$$\tan(\theta) = \frac{2I_2 - 2I_4}{2I_3 - I_1 - I_5}. \tag{4}$$

This result follows from the following identity:

$$\tan\left(\frac{a+b}{2}\right) = \frac{\sin(a) + \sin(b)}{\cos(a) + \cos(b)}. \tag{5}$$

By averaging two offset 5-point measurements, the 6-point algorithm is derived. This process can be extended to produce any number of N-point averaging algorithms.[7] The 6-point and 7-point algorithms are

$$\tan(\theta) = \frac{3I_2 - 4I_4 - I_6}{4I_3 - I_1 - 3I_5}, \tag{6}$$

$$\tan(\theta) = \frac{4I_2 - 8I_4 + 4I_6}{I_1 - 7I_3 + 7I_5 - I_7}, \tag{7}$$

The N-point averaging formulas can be expressed as follows:

$$\tan(\theta_m + \varepsilon) = \frac{-\sum_{n=1}^{N} I_n W_n \sin(\varphi_{n,m})}{\sum_{n=1}^{N} I_n W_n \cos(\varphi_{n,m})}, \tag{8}$$

where

$$\varphi_{n,m} = \varphi_n - \varphi_m = (n - m)\,\frac{\pi}{2}. \tag{9}$$

In the above formula, θ_m is the phase being determined, and ε is the error in the calculation. N is the number of points in the algorithm, and I_n, W_n, and $\varphi_{n,m}$ are the measured intensity, algorithm weighting coefficient, and relative spatial carrier phase at point n, respectively. Solving Eq. (8) for $\tan(\varepsilon)$ gives

$$\tan(\varepsilon) = \frac{\mathrm{num}_{(8)} \cos(\theta_m) - \mathrm{den}_{(8)} \sin(\theta_m)}{\mathrm{den}_{(8)} \cos(\theta_m) + \mathrm{num}_{(8)} \sin(\theta_m)}, \tag{10}$$

where

$$\mathrm{num}_{(8)} = -\sum_{n=1}^{N} I_n W_n \sin(\varphi_{n,m}), \tag{11}$$

$$\mathrm{den}_{(8)} = \sum_{n=1}^{N} I_n W_n \cos(\varphi_{n,m}). \tag{12}$$

$\mathrm{Num}_{(8)}$ and $\mathrm{den}_{(8)}$ are the numerator and the denominator of Eq. (8). The intensity of the measured interferogram can be expressed as

$$I_n = I_{\mathrm{avg}}[1 + \gamma \cos(\theta_n + \varphi_n)], \tag{13}$$

where I_{avg} and γ are the interferogram average intensity and visibility, respectively. Let θ_n be expressed as

$$\theta_n = \theta_m + \Delta_{n,m}, \tag{14}$$

where $\Delta_{n,m}$ is the difference between the phase at point (n), θ_n, and the phase determined by the calculation, θ_m. Substituting the value of θ_n from Eq. (14) into Eq. (13) and setting I_{avg} and γ equal to 1 gives

$$I_n = 1 + \cos(\theta_m + \varphi_m + \Delta_{n,m} + \varphi_{n,m}). \tag{15}$$

From Eq. (15), it should be evident that $\Delta_{n,m}$ represents a wavefront dependent phase shifting error. Using this value for I_n in Eq. (11) and expanding trigonometric terms give

$$\begin{aligned}\mathrm{num}_{(8)} = &-\sum_{n=1}^{N} W_n \frac{1}{2} \cos(\theta_m + \varphi_m + \Delta_{n,m}) \sin(2\varphi_{n,m}) \\ &+ \sum_{n=1}^{N} W_n \sin(\theta_m + \varphi_m + \Delta_{n,m}) \sin^2(\varphi_{n,m}) \\ &- \sum_{n=1}^{N} W_n \sin(\varphi_{n,m}).\end{aligned} \tag{16}$$

Since $\varphi_{n,m}$ is an integer multiple of $\pi/2$, then

$$\sin(2\varphi_{n,m}) = 0. \tag{17}$$

Equation (17) holds for all (n, m), and therefore the first sum in Eq. (16) is zero. The third sum in Eq. (16) is equal to either the sum of the odd weighting factors, or the even weighting factors, with the sign of the factors alternating. For example, using the 7-point algorithm weighting factors, the (alternating sign) odd factor sum is

$$\sum_{j=1}^{4} (-1)^j W_{2j-1} = 1 - 7 + 7 - 1 = 0. \tag{18}$$

The (alternating sign) even weighting factor sum is

$$\sum_{j=1}^{3} (-1)^j W_{2j} = -\,4 + 8 - 4 = 0. \tag{19}$$

The results of Eqs. (18) and (19) apply to all the N-point averaging algorithms and result from the symmetrical nature of the weighting factors. Therefore the third term in Eq. (16) is also zero giving

$$\mathrm{num}_{(8)} = \sum_{n=1}^{N} W_n \sin(\theta_m + \varphi_m + \Delta_{n,m}) \sin^2(\varphi_{n,m}). \tag{20}$$

In a similar manner, Eqs. (12) and (15) can be reduced to

$$\mathrm{den}_{(8)} = \sum_{n=1}^{N} W_n \cos(\theta_m + \varphi_m + \Delta_{n,m}) \cos^2(\varphi_{n,m}). \tag{21}$$

Finally, combining Eqs. (10), (20), and (21), and reducing gives

$$\tan(\varepsilon_m) = \frac{\sum_1 - \left[\sum_2 \cos(2\theta_m) + \sum_3 \sin(2\theta_m)\right]\cos(2\varphi_m)}{\sum_4 + \left[\sum_3 \cos(2\theta_m) - \sum_2 \sin(2\theta_m)\right]\cos(2\varphi_m)},$$

$$\sum_1 = \sum_{n=1}^{N} W_n \sin(\Delta_{n,m}),$$

$$\sum_2 = \sum_{n=1}^{N} W_n \cos(2\varphi_{n,m}) \sin(\Delta_{n,m}),$$

$$\sum_3 = \sum_{n=1}^{N} W_n \cos(2\varphi_{n,m})\cos(\Delta_{n,m}),$$

$$\sum_4 = \sum_{n=1}^{N} W_n \cos(\Delta_{n,m}). \quad (22)$$

Equation (22), the general error equation, expresses the phase calculation error in an N-point averaging algorithm as a function of the wavefront phase, θ_m, the carrier phase, φ_m, the algorithm weighting factors, W_n, and the wavefront phase deviation about the point of calculation, $\Delta_{n,m}$. This formula is also applicable to temporal phase shifting. In this case, $\Delta_{n,m}$ is the phase shifting error between steps n and m. The general error formula is very similar to one derived by Schwider *et al.*[3] for use with the synchronous detection algorithm. In his derivation, the assumption that $\Delta_{n,m} \ll 1$ was made and $\cos(\Delta_{n,m})$ and $\sin(\Delta_{n,m})$ were approximated to first order. Under these conditions and with $N = 4$, the general error formula will reduce to that of Schwider.

3. The 5-Point Algorithm: Wavefront with Tilt

As an example use of the general error formula, the phase calculation error for the 5-point algorithm will be determined for a wavefront with tilt. The results will then be compared with those obtained from a computer simulation. The first step is to evaluate the sums given in Eqs. (22). The weighting factors in the 5-point formula are $W_m = \{1, 2, 2, 2, 1\}$. If the phase is evaluated at the center point, $m = 3$, and $\varphi_{n,m} = \{-\pi, \pi/2, 0, \pi/2, \pi\}$. Let the wavefront tilt have a value of (t) radians/pixel in the direction of the spatial carrier. In this case, $\Delta_{n,m} = \{-2t, -t, 0, t, 2t\}$. Using the values given above, the sum terms of Eq. (22) are evaluated as follows:

$$\sum_1 = \sum_{n=1}^{N} W_n \sin(\Delta_{n,m}) = 0, \quad (23)$$

$$\sum_2 = \sum_{n=1}^{N} W_n \cos(2\varphi_{n,m})\sin(\Delta_{n,m}) = 0, \quad (24)$$

$$\sum_3 = \sum_{n=1}^{N} W_n \cos(2\varphi_{n,m})\cos(\Delta_{n,m}) = -8\cos(t)\sin^2(t/2), \quad (25)$$

$$\sum_4 = \sum_{n=1}^{N} W_n \cos(\Delta_{n,m}) = 8\cos(t)\cos^2(t/2). \quad (26)$$

Using the sums given in Eqs. (23)–(26), Eq. (22) becomes

$$\tan(\varepsilon_m) = \frac{\sin^2(t/2)\sin(2\theta_m)\cos(2\varphi_m)}{\cos^2(t/2) - \sin^2(t/2)\cos(2\theta_m)\cos(2\varphi_m)}. \quad (27)$$

A plot of Eq. (20) with $t = \pi/64$ radians/pixel is shown in Fig. 2.

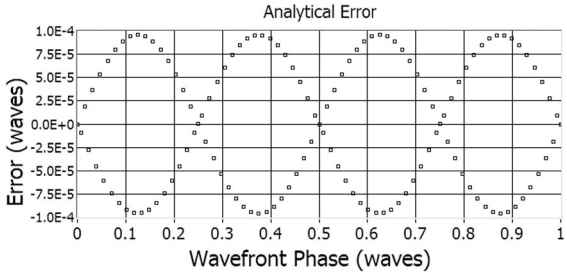

Fig. 2. The 5-point algorithm theoretical phase calculation error for a wavefront with tilt. $t = \pi/64$ rad/pix. Values calculated with Eq. (20).

As pointed out by several authors,[7,9,15] the phase dependence of the error envelope is proportional to $\sin(2\theta)$, with the error oscillating in sign at twice the carrier frequency. Maximizing Eq. (27) with respect to θ, the theoretical maximum error is found to be

$$\tan(\varepsilon)_{\max} = \frac{\sin^2(t/2)}{\sqrt{\cos(t)}}. \quad (28)$$

Using Eq. (28) the peak-to-valley (Pk–v) error in waves is

$$\varepsilon_{\text{Pk-v}} = \frac{1}{\pi}\arctan\left(\frac{\sin^2(t/2)}{\sqrt{\cos(t)}}\right). \quad (29)$$

Using $t = \pi/64$ in Eq. (29) gives a theoretical Pk–v error of 1.91825×10^{-4} waves that corresponds with the Pk–v error in Fig. 2. Several authors have noted the relationship of the peak-to-valley error with the square of a linear phase shift miscalibration for the 5-point algorithm.[9,15] This dependence is true for small tilt angles and can be shown by approximating Eq. (29) as

$$\varepsilon_{\text{Pk–v}} \approx \frac{1}{\pi}\left(\frac{t}{2}\right)^2. \quad (30)$$

A computer simulation was also conducted. Phase values were calculated on a 512×512 array for a wavefront with $t = \pi/64$ rad/pixel in the x direction. A spatial carrier phase of $\pi/2$ rad/pixel in the x direction was added to the tilt phase, and the interferogram intensity values at each point in the array were calculated using Eq. (6) with I_{avg} and γ set equal to one. Using the generated intensity values, the 5-point algorithm was then used to calculate the phase at each point in the array. The actual phase was then subtracted from the calculated phase to obtain the phase calculation error. The results of the simulation are shown in Fig. 3. As can be seen by comparing Figs. 2 and 3, the two plots are visibly identical with a maximum difference between corresponding points of 10^{-8} waves.

4. *N*-Point Algorithm: Wavefront with Tilt

The general error formula, Eq. (15), can be reduced in the case of a wavefront with tilt to the following form:

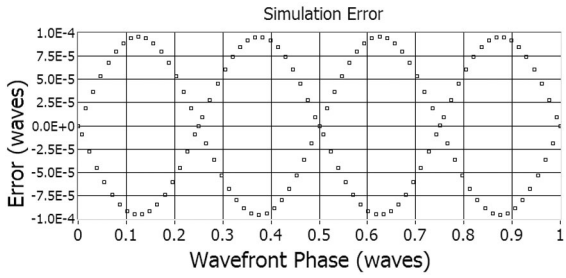

Fig. 3. The 5-point algorithm phase calculation error for a wavefront with tilt. $t = \pi/64$ rad/pix. Values obtained through computer simulation.

N even

$$\tan(\varepsilon) = \frac{\sin(t/2)^{N-3}\cos(2\theta)\cos(2\varphi)}{\cos(t/2)^{N-3} + \sin(t/2)^{N-3}\sin(2\theta)\cos(2\varphi)},$$

N odd

$$\tan(\varepsilon) = \frac{\sin(t/2)^{N-3}\sin(2\theta)\cos(2\varphi)}{\cos(t/2)^{N-3} + \sin(t/2)^{N-3}\cos(2\theta)\cos(2\varphi)}, \quad (31)$$

The maximum error for both even and odd N is determined by maximizing Eqs. (31) with respect to θ. The maximum error for both even and odd N is given by

$$\tan(\varepsilon)_{\max} = \frac{\sin(t/2)^{N-3}}{\sqrt{\cos(t/2)^{2(N-3)} - \sin(t/2)^{2(N-3)}}}. \quad (32)$$

Using Eq. (32) the peak-to-valley error in waves for a wavefront with tilt is

$$\varepsilon_{\mathrm{Pk-v}} = \frac{1}{\pi}\arctan\left(\frac{\sin(t/2)^{N-3}}{\sqrt{\cos(t/2)^{2(N-3)} - \sin(t/2)^{2(N-3)}}}\right). \quad (33)$$

For small t, Eq. (33) may be approximated as

$$\varepsilon_{\mathrm{Pk-v}} = \frac{1}{\pi}\arctan[\tan(t/2)^{N-3}]. \quad (34)$$

Using Eq. (33), the theoretical peak-to-valley error as a function of tilt for $N = 4$, 5, 6, and 7 was plotted and is shown as the solid curves in Fig. 4. Note that 0.25 wave per pixel corresponds to the sampling Nyquist frequency. A computer simulation was also conducted with the results shown as points along the theoretical curves. Any discrepancies between the theoretical values and those obtained through simulation are due to the fact that the simulation wavefront sample points may not fall at the exact phase necessary for a maximum in the calculation error. A general analytical formula for linear phase shift errors valid for all phase shifting algorithms without restriction to the phase increment has been published by de Groot.[16] His formula is elegantly

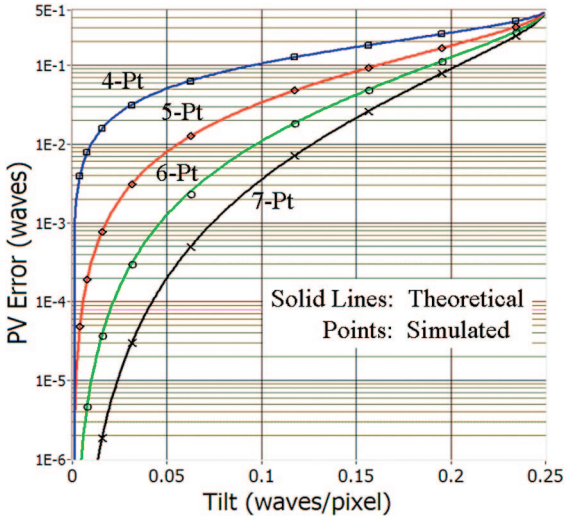

Fig. 4. (Color online) Peak-to-valley phase calculation error as a function of wavefront tilt for the 4-, 5-, 6-, and 7-point algorithms. The solid curves represent the theoretical values determined with Eq. (33). The points indicate values obtained via computer simulation.

derived in terms of a windowed discrete Fourier transform of the wavefront intensity. In the case of a wavefront with tilt, the above results can be derived from de Groot's formula.

5. Pixelated Spatial Carrier

Tilt fringes are generally used to produce a linear spatial carrier. When the carrier fringe spacing is 4 pixels wide, there is a relative phase shift of $\pi/2$ between pixels. A portion of a linear carrier is shown in Fig. 5 (top) with the carrier phase at each pixel given in degrees. Upon interference with the test wavefront, this linear carrier will become modulated; that is, the relative phase shift between pixels will no longer be 90°. To calculate the phase at the center pixel, the 5-point formula can be used. The error in this phase calculation results directly from the wave-

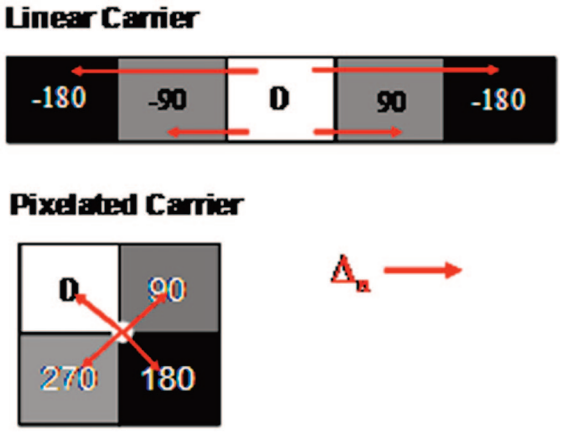

Fig. 5. (Color online) Linear versus pixelated spatial carrier. The arrows represent the phase shift error associated with the wavefront being measured. The pixelated spatial carrier groups four phase shifted pixels about a center point in order to minimize accumulative phase shift error.

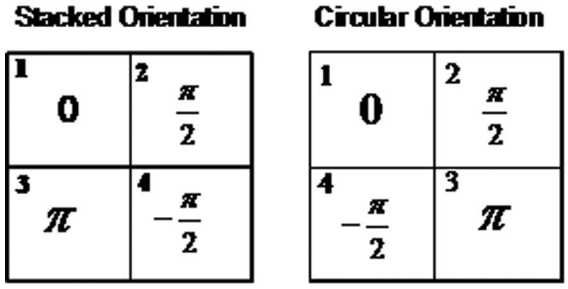

Fig. 6. Stacked and circular pixelated mask orientations.

front induced phase shift errors, Δ_n, shown as arrows in Fig. 5. One way to minimize these errors is to minimize the distance between the point at which the phase is being calculated and all other points involved in the calculation. The pixelated spatial carrier shown in Fig. 5 (bottom) accomplishes this by grouping the phase shifted pixels together around a single point in two dimensions, minimizing the phase shift change due to the spatial variation in the test wavefront. Physical implementation of the pixelated spatial carrier has been well covered by other authors[14,17] and is not discussed in this paper. In the remainder of this section, two different pixelated spatial carrier orientations are introduced, each having an associated 4-point and 9-point algorithm. The applicability of the generalized error formula, Eq. (22), is shown, and a comparison of algorithm performance for a wavefront with tilt is made.

The two orientations of the pixelated spatial carrier are shown in Fig. 6. The first is called the stacked orientation, since pixels phase shifted by 180° are stacked one over the other. The second is called the circular orientation, since the spatial carrier increases in a right-hand circular fashion. The circular-4 and stacked-4 algorithms are simply the standard 4-point linear algorithm, Eq. (1), used with the circular and stacked pixelated mask orientations.

The 9-point algorithms were developed by noting that each pixel is contained within four separate groupings of phase shifted pixels, and each grouping of pixels can be used to determine the phase with the appropriate 4-point algorithm. Figure 7 shows a 4 × 4 section of a circular pixelated mask spatial carrier, with the pixels in the lower right section labeled 1–9. The phase at the center pixel, 5, can be determined with the 4-point algorithm using points (1, 2, 5, 4), (2, 3, 6, 5), (4, 5, 8, 7), or (5, 6, 9, 8). Since there is a relative phase offset of $\pi/2$ between each of these phase calculations, an averaging of the results will significantly reduce the calculation error. This is completely analogous to the technique for deriving the N-point averaging algorithms from the 4-point algorithm as discussed in Section 2. Additionally, as was also pointed out in Section 2, instead of making four separate measurements and then combining the results, the numerators and the denominators of each of 4-point calculations can be combined to give a single 9-point formula. The same technique is

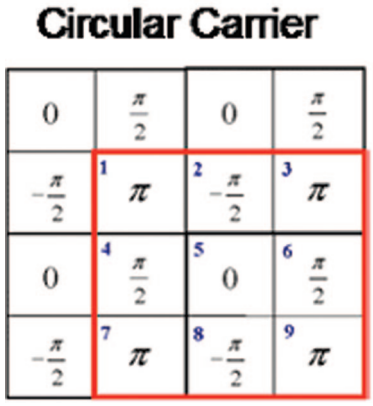

Fig. 7. (Color online) A 4 × 4 section of a circular pixelated mask carrier. The phase at point-5 can be calculated using the intensity values obtained at pixels 1–9 in the circular-9 algorithm.

used with the stacked carrier to derive the stacked-9 algorithm. The circular-9 formula is

$$\tan[\theta_5] = \frac{2(I_2 + I_8 - I_4 - I_6)}{-I_1 - I_3 + 4I_5 - I_7 - I_9}. \tag{35}$$

The stacked-9 formula is

$$\tan[\theta_5] = \frac{I_1 + I_3 - 2I_4 - 2I_6 + I_7 + I_9}{-2I_2 + 4I_5 - 2I_8}. \tag{36}$$

Since the circular-4 and stacked-4 algorithms are both equal to the standard linear-4 algorithm given in Eq. (1), the general error formula of Eq. (22) is applicable. Note that the only difference among the linear-4, circular-4, and stacked-4 algorithms is the spatial orientation of the phase shifted pixels that results in different set of Δ_n's, and therefore a different calculation error for each algorithm. In Section 2, the numerator, Eq. (16), of the general error formula was significantly simplified due to the fact that the first and third sums were shown to be equal to zero. This is also true in the case of the circular-9 and stacked-9 algorithms. A similar relation holds for the denominator terms of the general error formula. Therefore the general error formula is applicable to both the circular-9 and stacked-9 algorithms.

Using the general error formula, the phase calculation error of the stack-4 algorithm for a wavefront with tilt is given by

$$\tan(\varepsilon) = \frac{\sin(t_x/2)\cos(2\theta)\cos(2\varphi)}{\cos(t_x/2) + \sin(t_x/2)\sin(2\theta)\cos(2\varphi)}, \tag{37}$$

where t_x is the component of tilt in the x direction. The maximum error amplitude is given by

$$\tan(\varepsilon)_{\max} = \frac{\sin(t_x/2)}{\sqrt{\cos(t_x)}}. \tag{38}$$

This is equivalent to the linear-4 algorithm error.

The circular-4 algorithm error is given by

$$\tan(\varepsilon) = \frac{-\sin(t_x/2)\sin(t_y/2)\sin(2\theta)\cos(2\varphi)}{\cos(t_x/2)\cos(t_y/2) - \sin(t_x/2)\sin(t_y/2)\cos(2\theta)\cos(2\varphi)}. \tag{39}$$

The circular-4 error maximum amplitude is

$$\tan(\varepsilon)_{\max} = \frac{\sqrt{2}\,\sin(t_x/2)\sin(t_y/2)}{\sqrt{\cos(t_x) + \cos(t_y)}} \tag{40}$$

where t_x and t_y are the components of tilt in the x and y directions, respectively. A tilt orientation of 45° will produce the maximum error. In this case, the maximum error amplitude is given by

$$\tan(\varepsilon)_{\max} = \frac{\sin^2(t_x/2)}{\sqrt{\cos(t_x)}}, \tag{41}$$

which is equal to the maximum error in the linear-5 algorithm, Eq. (28). The stacked-9 algorithm error is given by

$$\tan(\varepsilon) = \frac{-\sin^2(t_x/2)\cos(2\theta)\cos(2\varphi)}{\cos^2(t_x/2) + \sin^2(t_x/2)\sin(2\theta)\cos(2\varphi)}. \tag{42}$$

This error is equal to the error in the linear-5 algorithm and therefore has the same maximum error as shown in Eq. (41). The circular-9 algorithm error is given by

$$\tan(\varepsilon) = \frac{-\sin^2(t_x/2)\sin^2(t_y/2)\sin(2\theta)\cos(2\varphi)}{\cos^2(t_x/2)\cos^2(t_y/2) + \sin^2(t_x/2)\sin^2(t_y/2)\cos(2\theta)\cos(2\varphi)}. \tag{43}$$

The circular-9 maximum error amplitude is

$$\tan(\varepsilon)_{\max} = \frac{\sin^2(t_x/2)\sin^2(t_y/2)}{\sqrt{\cos^4(t_x/2)\cos^4(t_y/2) - \sin^4(t_x/2)\sin^4(t_y/2)}}. \tag{44}$$

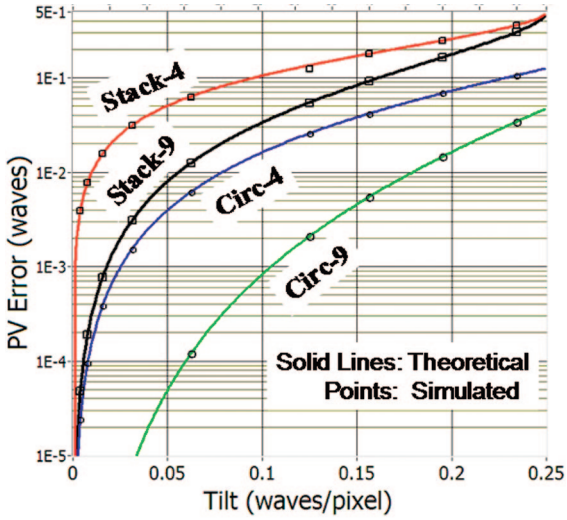

Fig. 8. (Color online) Peak-to-valley phase calculation error as a function of wavefront tilt for the circular-4, stacked-4, circular-9, and stacked-9 algorithms. The solid curves represent theoretical values. Points indicate values obtained via computer simulation. Tilt orientation is at 0° and 45° for the stacked and circular algorithms, respectively.

Similar to the circular-4 case, a tilt orientation of 45° will produce the maximum error. Setting $t_x = t_y$ in Eq. (44) gives

$$\tan(\varepsilon)_{\max} = \frac{\sin^4(t_x/2)}{\sqrt{\cos^8(t_x/2) - \sin^8(t_x/2)}}. \tag{45}$$

This error is equivalent to the linear-7 algorithm error for a wavefront with tilt at a 45° orientation.

The maximum peak-to-valley theoretical errors for the circular and stacked (4- and 9-point) algorithms as functions of wavefront tilt are plotted and shown as the solid curves in Fig. 8. To make a comparison of maximum error, the circular algorithms are shown for a tilt orientation of 45°, and the stacked algorithms are shown at a tilt orientation of zero. A computer simulation was also conducted with the results shown as points along the theoretical curves. It is obvious that the circular-9 formula has the best performance. A concern with this comparison is that in going from the 4-point to the 9-point formula, the lateral resolution of the calculated phase map will suffer. It is true that the lateral resolution of the 9-point formula will be less than that of the 4-point formula, but it turns out that the differences are insignificant when compared to the loss in resolution

Table 1. Spatial Carrier Phase Shifting Calculation Error for a Wavefront with Tilt

Algorithm	$\mathrm{Tan}(\varepsilon)$	$\mathrm{Tan}(\varepsilon)_{\max}$	Comment
Linear-N N-even	$\dfrac{\sin(t_x/2)^{N-3}\cos(2\theta)\cos(2\varphi)}{\cos(t_x/2)^{N-3}+\sin(t_x/2)^{N-3}\sin(2\theta)\cos(2\varphi)}$	$\dfrac{\sin(t_x/2)^{N-3}}{\sqrt{\cos(t_x/2)^{2(N-3)}-\sin(t_x/2)^{2(N-3)}}}$	$N \geq 4$
Linear-N N-odd	$\dfrac{\sin(t_x/2)^{N-3}\sin(2\theta)\cos(2\varphi)}{\cos(t_x/2)^{N-3}-\sin(t_x/2)^{N-3}\cos(2\theta)\cos(2\varphi)}$	$\dfrac{\sin(t_x/2)^{N-3}}{\sqrt{\cos(t_x/2)^{2(N-3)}-\sin(t_x/2)^{2(N-3)}}}$	$N \geq 4$
Linear-4	$\dfrac{\sin(t_x/2)\cos(2\theta)\cos(2\varphi)}{\cos(t_x/2)+\sin(t_x/2)\sin(2\theta)\cos(2\varphi)}$	$\dfrac{\sin(t_x/2)}{\sqrt{\cos(t_x)}}$	
Linear-5	$\dfrac{\sin^2(t_x/2)\sin(2\theta)\cos(2\varphi)}{\cos^2(t_x/2)-\sin^2(t_x/2)\cos(2\theta)\cos(2\varphi)}$	$\dfrac{\sin^2(t_x/2)}{\sqrt{\cos(t_x)}}$	
Linear-6	$\dfrac{\sin^3(t_x/2)\cos(2\theta)\cos(2\varphi)}{\cos^3(t_x/2)+\sin^3(t_x/2)\sin(2\theta)\cos(2\varphi)}$	$\dfrac{\sin^3(t_x/2)}{\sqrt{\cos^6(t_x/2)-\sin^6(t_x/2)}}$	
Linear-7	$\dfrac{\sin^4(t_x/2)\sin(2\theta)\cos(2\varphi)}{\cos^4(t_x/2)-\sin^4(t_x/2)\cos(2\theta)\cos(2\varphi)}$	$\dfrac{\sin^4(t_x/2)}{\sqrt{\cos^8(t_x/2)-\sin^8(t_x/2)}}$	
Stacked-4	$\dfrac{\sin(t_x/2)\cos(2\theta)\cos(2\varphi)}{\cos(t_x/2)+\sin(t_x/2)\sin(2\theta)\cos(2\varphi)}$	$\dfrac{\sin(t_x/2)}{\sqrt{\cos(t_x)}}$	Equal to linear-4
Circular-4	$\dfrac{-\sin(t_x/2)\sin(t_y/2)\sin(2\theta)\cos(2\varphi)}{\cos(t_x/2)\cos(t_y/2)-\sin(t_x/2)\sin(t_y/2)\cos(2\theta)\cos(2\varphi)}$	$\dfrac{\sqrt{2}\sin(t_x/2)\sin(t_y/2)}{\sqrt{\cos(t_x)+\cos(t_y)}}$	Equal to linear-5 for tilt orientation of 45°
Stacked-9	$\dfrac{-\sin(t_x/2)\cos(2\theta)\cos(2\varphi)}{\cos(t_x/2)-\sin(t_x/2)\sin(2\theta)\cos(2\varphi)}$	$\dfrac{\sin^2(t_x/2)}{\sqrt{\cos(t_x)}}$	Equal to linear-5
Circular-9	$\dfrac{-\sin(t_x/2)\sin(t_y/2)\sin(2\theta)\cos(2\varphi)}{\cos(t_x/2)\cos(t_y/2)+\sin(t_x/2)\sin(t_y/2)\cos(2\theta)\cos(2\varphi)}$	$\dfrac{\sin^2(t_x/2)\sin^2(t_y/2)}{\sqrt{\cos^4(t_x/2)\cos^4(t_y/2)+\sin^4(t_x/2)\sin^4(t_y/2)}}$	Equal to linear-7 for tilt orientation of 45°

resulting from the limiting aperture of the interferometers imaging system. An additional concern with the use of the circular-9 algorithm relates to the issue of camera smear.[18] When using a sensor with 50% smear, the stacked algorithm outperforms the circular algorithm for low values of tilt. However, since the circular algorithm's performance is so much better than that of the stacked algorithm, it is better to simply eliminate the smear through shuttering the laser than to use the lower performing algorithm. A summary of the error formula for both the linear and the pixelated spatial carrier algorithms is provided in Table 1.

6. Summary

The pixelated mask spatial carrier technique has been introduced, and the circular-4, stacked-4, circular-9, and stacked-9 algorithms presented. To allow comparisons of algorithm performance, a generalized error formula was derived for the wavefront induced phase calculation error. The generalized error formula was derived for the linear averaging algorithms and was then shown to be applicable to the spatial carrier algorithms. The generalized error formula was simplified for the case of a wavefront with tilt, and the results for both the linear and the pixelated spatial carrier algorithms were compared with those obtained through computer simulation. The performances of the stacked-4 and the stacked-9 algorithms, when measuring a wavefront with tilt, were found to be equivalent to those of the linear-4 and linear-5 algorithms, respectively. The maximum error for the circular-4 algorithm is approximately ½ that of the linear-5 algorithm, and the maximum error in the circular-9 algorithm is approximately ¼ that of the linear-7 algorithm. In all cases, the phase calculation error when measuring a wavefront with tilt is strictly phase dependent; that is, the first sum of the general error equation is zero and the numerator of the general error equation contains a $\sin(2\theta)$ or $\cos(2\theta)$ term. Due to vibration, the absolute phase of the wavefront under test may move around by as much as a few waves, which results in the phase of the error moving around due to the 2θ dependence. In this case, if several measurements are made and then averaged, the resulting error can be averaged to near zero. This error averaging technique is successfully employed in 4D technology interferometers.[14] On a final note, for nonlinear wavefronts, analytic solutions to the general error formula have proved illusive; however, assuming wavefronts with small deviations, good approximations can be derived. The most significant difference between wavefronts with tilt and those with nonlinear deviations results from the fact that the first term in the general error equation is no longer zero. The error in the phase calculation for nonlinear wavefronts contains a nonphase dependent offset that is proportional to the local slope

of the wavefront being measured for the linear and pixelated 4-point algorithms. The offset is proportional to the curvature of the wavefront for the linear algorithms with $N > 4$, and the stacked-9 and circular-9 algorithms.

References

1. D. Malacara, M. Servin, and Z. Malacara, *Interferogram Analysis for Optical Testing* (Marcel Dekker, 1998).
2. D. Malacara, *Optical Shop Testing,* 2nd ed. (Wiley, 1992).
3. J. Schwider, R. Burow, K. E. Elssner, J. Grzanna, R. Spolaczyk, and K. Merkel, "Digital wave-front measuring interferometry: some systematic error sources," Appl. Opt. **22,** 3421–3432 (1983).
4. K. Hibino, B. F. Oreb, D. I. Farrant, and K. G. Larkin, "Phase shifting for nonsinusoidal waveforms with phase-shift errors," J. Opt. Soc. Am. A **12,** 761–768 (1995).
5. K. G. Larkin and B. F. Oreb, "Design and assessment of symmetrical phase-shifting algorithms," J. Opt. Soc. Am. A **9,** 1740–1748 (1992).
6. D. W. Phillion, "General methods for generating phase-shifting interferometry algorithms," Appl. Opt. **36,** 8098–8115 (1997).
7. J. Schmit and K. Creath, "Extended averaging technique for derivation of error-compensating algorithms in phase-shifting interferometry," Appl. Opt. **34,** 3610–3619 (1995).
8. M. Servin, D. Malacara, J. L. Marroquin, and F. J. Cuevas, "Complex linear filters for phase shifting with very low detuning sensitivity," J. Mod. Opt. **44,** 1269–1278 (1997).
9. Y. Surrel, "Phase stepping: a new self-calibrating algorithm," Appl. Opt. **32,** 3598–3600 (1993).
10. R. Jozwicki, M. Kujawinska, and L. A. Salbut, "New contra old wavefront measurement concepts for interferometric optical testing," Opt. Eng. **31,** 422–433 (1992).
11. M. Takeda, H. Ina, and S. Kobayashi, "Fourier-transform method of fringe-pattern analysis for computer-based topography and interferometry," J. Opt. Soc. Am. **72,** 156–160 (1982).
12. D. M. Shough, O. Y. Kwon, and D. F. Leary, "High speed interferometric measurement of aerodynamic phenomena," in *Propagation of High-Energy Laser Beams Through the Earth's Atmosphere*, P. B. Ulrich and L. E. Wilson, eds., Proc. SPIE **1221,** 394–403 (1990).
13. K. Creath and J. Schmit, "Errors in spatial phase-stepping techniques," in *Interferometry '94: New Techniques and Analysis in Optical Measurements*, M. Kujawinska and K. Patorski, eds., Proc. SPIE **2340,** 170–176 (1994).
14. J. E. Millerd, N. J. Brock, J. B. Hayes, M. B. North-Morris, M. Novak, and J. C. Wyant, "Pixelated phase-mask dynamic interferometer," in *Interferometry XII: Techniques and Analysis*, K. Creath and J. Schmit, eds., Proc. SPIE **5531,** 304–314 (2004).
15. P. Hariharan, B. F. Oreb, and T. Eiji, "Digital phase-shifting interferometry: a simple error-compensating phase calculation algorithm," Appl. Opt. **26,** 2504–2505 (1987).
16. P. de Groot, "Phase-shift calibration errors in interferometers with spherical Fizeau cavities," Appl. Opt. **34,** 2856–2863 (1995).
17. J. D. Tobiason and K. W. Atherton, "Interferometer using integrated imaging array and high-density polarizer array," US Patent 6,850,329 (1 February 2005).
18. J. E. Millerd, N. J. Brock, J. B. Hayes, M. B. North-Morris, B. T. Kimbrough, and J. C. Wyant, "Pixelated phase-mask dynamic interferometers," in *Fringe 2005* (Springer, 2005), pp. 640–647.